Comparison of the slag rim formation of two different mold powders

I. Marschall, N. Kölbl, H. Harmuth
University of Leoben, Leoben, Austria

Keywords: mold powder, slag rim, casting, steel

Abstract

Two fluorine containing mold powders with a SiO_2 content of 37.0 mass% and 17.3 mass% were characterized concerning their slag rim formation behavior. Both were in contact with high-aluminum-containing steel. Under service conditions, significant differences in slag rim size have been observed from both mold powders.

The melting and solidification of these original powders have been defined by simultaneous thermal analysis. The viscosity at 1300°C and the break temperature were determined by a rotary viscometer. In addition, quench tests were performed in the range of 500°C-1200°C. These results were compared with the structure of the polished cross sections of the slag rim samples.

It was concluded that the size of the slag rims is influenced by the melting range of the mold powders. Due to the alumina pick-up of the slag, cuspidine was not the dominating mineral phase in the crystallized parts of the rims.

Introduction

In casting operation employing mold powders usually a crust on the mold in the meniscus region called slag rim is formed. This slag rim is attached to the copper mold and moves with the mold oscillation [1]. Its thickness has a strong impact on heat flux and a large influence on the initial shell formation. In order to achieve steady state condition of the solidification process and the desired surface quality the size the slag rim should be stable and robust during the whole casting [2,3]. It is mentioned, that during the upward mold motion, the bottom part of the slag rim is coated by liquid and solid powder. During the downward mold motion, this new powder layer melts when coming into contact with the hot steel meniscus. Thus the infiltrated slag layer and the bottom part of the rim are renewed [4, 5, 6]. Mold slag lubrication (viscosity and liquid slag thickness), thermal properties of the mold slag (thermal conductivity, absorption) and the crystallization behavior of the mold slag are some of the most important variables to be controlled [3]

In the casting of high-alumina-containing grades, the mold powder chemistry that is attained in the mold may significantly differ from that of the original powder chemistry composition. In a previous investigation [7] the slag quickly changes its composition to a lower amount of silica and a higher content of alumina. Hence mold powders with increased Al_2O_3 contend were developed and characterized [7]. But so far no investigation has dealt with the influence of the Al_2O_3 increase on the slag rim formation.

Samples

In this study, two fluorine containing mold powders with different SiO_2 content of 37.0 and 17.3 mass% were characterized concerning their slag rim formation. Their chemical compositions are given in Table1. Remarkable is the MnO content of 6.5 mass% of powder A and the high Al_2O_3 content of 23.0 mass% of powder B.

Powder A is granulated and contains a soda lime glass as the main constituent. Further components are fluorite (CaF_2), wollastonite ($CaSiO_3$), cryolite (Na_3AlF_6), manganese carbonate ($MnCO_3$), quartz (SiO_2) and carbon (C). Powder B is granulated, too. Its main components are alumina (Al_2O_3), fluorite and soda lime glass. In minor amounts, phosphorus slag, consisting of cuspidine ($Ca_3Si_2O_7 \cdot CaF_2$), wollastonite and a glassy phase, villiaumite (NaF_2), lithium carbonate (Li_2CO_3) and carbon are present.

Table 1 Chemical composition of the mold fluxes

	F (mass%)	Na_2O (mass%)	MgO (mass%)	Al_2O_3 (mass%)	SiO_2 (mass%)	CaO (mass%)	Li_2O (mass%)	MnO (mass%)	C (mass%)	C/S
Powder A	10.0	10.8	1.1	3.8	37.0	24.6	2.1	6.5	5.0	0.55
Powder B	10.1	11.9	0.7	23.0	17.3	21.0	2.7	0.8	4.7	1.22

During tail out, after casting of high alumina alloyed steel grades, slag rim samples of both mold powders were taken. From Figure 1, it can be clearly seen that the slag rim formed from powder A is much smaller than the slag rim formed from powder B.

a) b)

Figure 1 Slag rims taken after service; a) powder A, b) powder B

Experimental

In a first step, a Simultaneous Thermal Analysis (STA) was carried out on the mold powder samples. 80 µg of the ground samples were heated to 1400°C with a heating rate of 5°Cmin^{-1}, soaked for 15 min and cooled down to room temperature with 10°Cmin^{-1}. In a next step, the melting behavior was characterized by quench tests. Therefore the powders were annealed at selected temperatures in a laboratory kiln under oxidizing conditions within steel crucibles. After 30 min dwell, the samples were quenched to room temperature within the crucibles. To investigate the solidification behaviour, the powders were decarburised, melted within 5 min at 1300°C in a platinum crucible in a first laboratory kiln and quenched to 900°C on a preheated steel plate in a second laboratory kiln. In the first run the dell time at 900 °C was

five minutes; in the second run 60 minutes have been chosen. Subsequently, all annealed specimens were mineralogically investigated. In addition, the viscosity of the powders was measured in oxidizing atmosphere with a rotary viscometer. The slag rim samples were cut, and the cross sections microscopically investigated.

Results

Characterization of the mold powders

Melting behavior

Resulting from the STA, the carbon combustion of both mold powders is comparable. It starts at about 395°C in the case of powder A and 380°C in the case of powder B. At 560°C the carbon combustion is finished In case of powder A liquid phase formation starts at about 680 °C, at 965 °C the powder is totally liquefied. Different results have been achieved for powder B, witch shows a begin of melting at 933°C and complete liquefaction at 1125°C.

The microscopic analysis (see Fig. 2) for powder A revealed that after heat treatment at 750°C the soda lime glass and cryolite were completely molten and formed a cohesive glass phase. Fluorite started melting, too. As a result, an intermediate phase, fluorpectolite ($NaCa_2Si_3O_8F$), was formed. The wollastonite crystals are surrounded by cuspidine. $MnCO_3$ was dissociated to MnO. After heat treatment at 900°C, residuals of fluorite and MnO are still present. Fluorpectolite was dissolved by the liquid. Instead, cuspidine was formed. After annealing at 1000°C, fluorite is the only detected mineral phase and after heat treatment at 1100°C the sample is totally glassy.

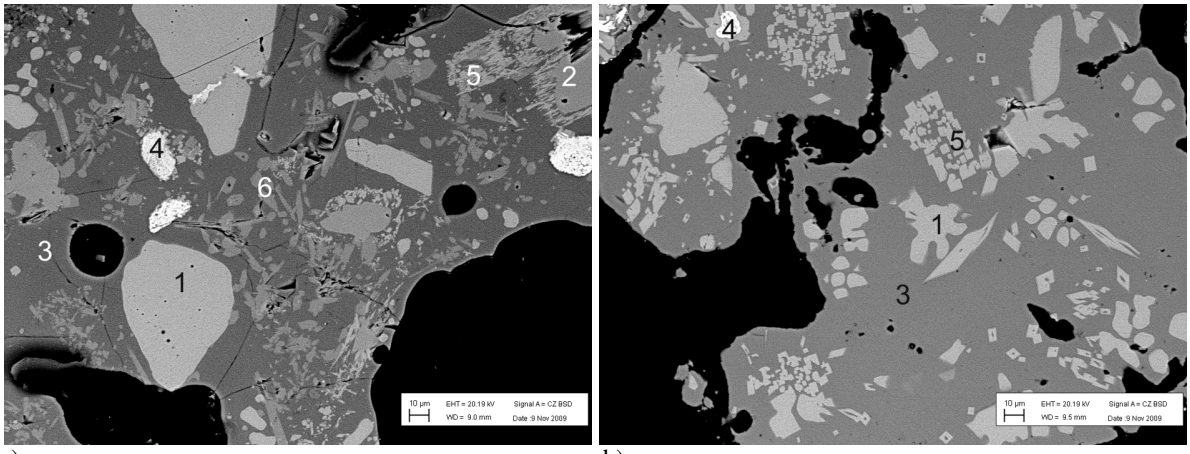

a) b)

Figure 2 Back scattered electron image of powder A after heat treatment, a) 750°C, b) 900°C; 1: fluorite, 2: wollastonite, 3: glassy phase, 4: MnO, 5: cuspidine, 6: flourpectolite

In case of powder B, soda lime glass together with the glassy phase from the phosphorus slag is again the first melting raw material, but due to the lower amount of the glassy phases no cohesive glass phase was formed after heat treatment at 750°C. In Figure 3 it can be seen that the spherical granules are still in shape. Fluorite and wollastonite reacted to form cuspidine at this temperature step. Even after heat treatment at 900°C, only low amounts of glassy phase could be

detected. These have reacted in liquid state with alumina to form a silicofluoride named phase1 in succession. Its composition is given in Table 2. Ti which was present within the alumina grains reacted with CaO to perovskite ($CaTiO_3$). $LiCO_3$ was dissociated and formed with fluorine LiF. After annealing at 1000°C the powder was sintered. Cuspidine, phase I and residuals of alumina are the dominating phases. Even after heat treatment at 1100°C, residuals of alumina and phase I are still present. After melting of cuspidine CaF_2 remained as a solid residue.

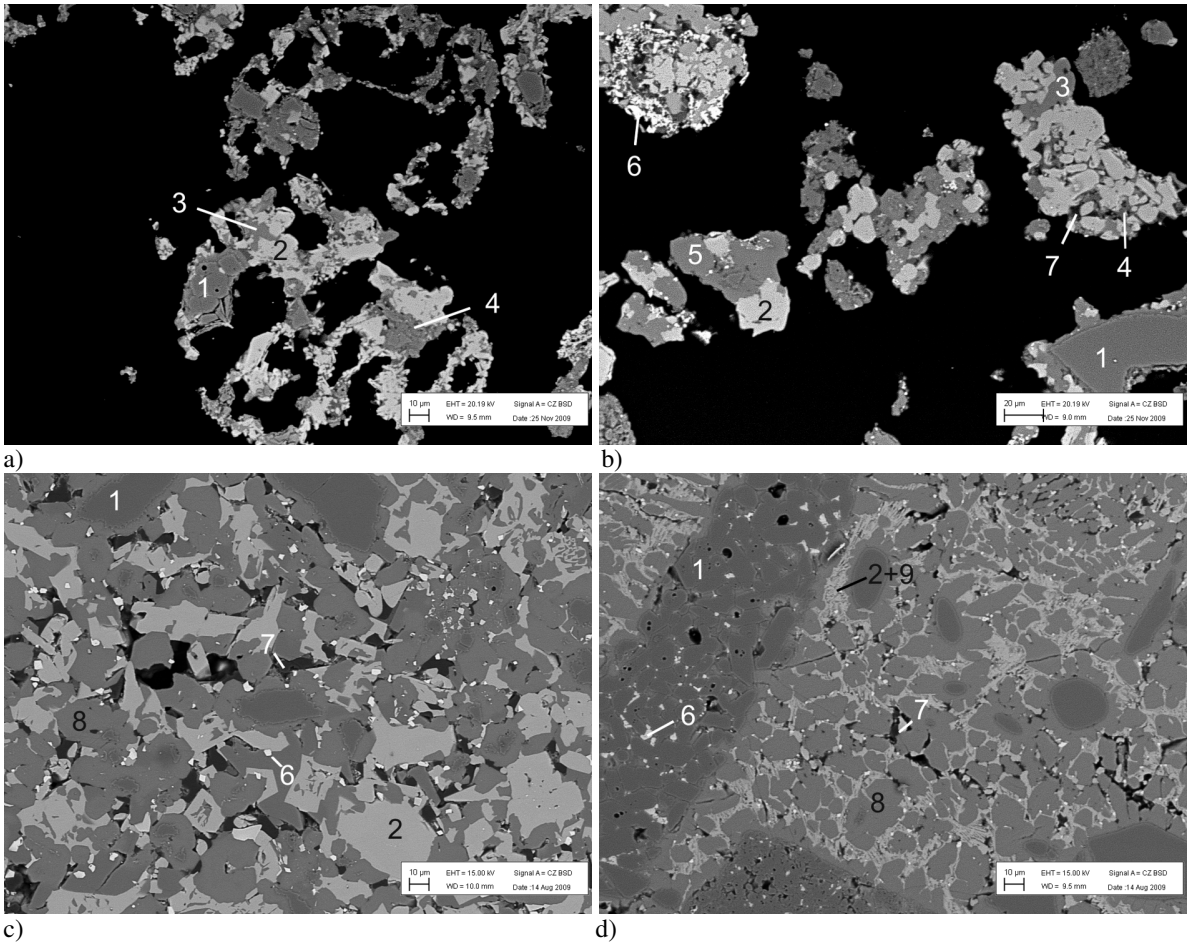

Figure 3 Back scattered electron image of powder B after heat treatment,
a) 750°C, b) 900°C, c) 1000°C, d) 1100°C;
1: alumina, 2: cuspidine, 3: glassy phase, 4: villiaumite 5: phase I at 900°C, 6: perovskite, 7: LiF, 8: phase I at 1000 and 1100°C, 9: fluorite

Table 2 Chemical composition of phases I in the original slag determined by energy dispersive microanalysis (EDX)

	F (mol%)	Na (mol%)	Ca (mol%)	Al mol%)	Si (mol%)	O (mol%)
heating 900°C	6	13	2	14	9	57
heating 1000°C and 1100°C	7	11	5	16	8	53
cooling 900°C	8	9	6	12	8	57

Solidification

The solidification of both mold powders differs. Whereas no crystallization was detected with powder A by DTA, by DTA, for powder B a first peak indicating crystallisation was observed at 1255°C. A further peak at 883°C is more intense. Resulting from the quench tests at 900°C after a dwell of 60min, low amounts of cuspidine and fluorite were present for powder A. Powder B formed small sized spherical pores during 5min dwell. Within this pores the crystallization of fluorite starts (see Figure 4). After 60min dwell phase I is the dominating phase. Its chemical composition is given in Table 2. Within the gussets cuspidine, fluorite, LiF and spinell were formed. In contact with the steel plate, gehlenite is present.

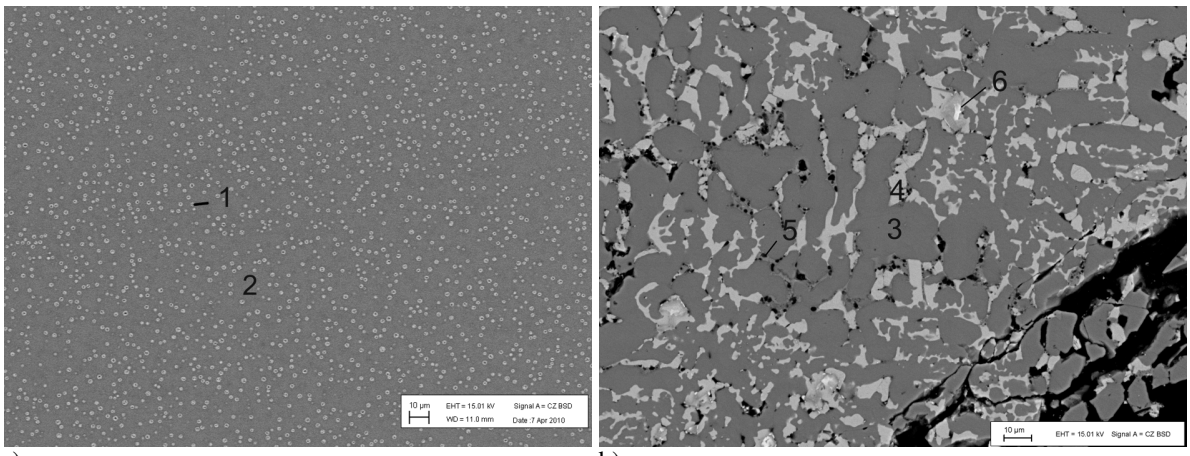

a) b)

Figure 4 Back scattered electron image of powder B after quenching from 1300°C to 900°C , a) 5 min dwell, b) 60 min dwell, 1: fluorite, 2: glassy phase, 3: phase I, 4: cuspidine and fluorite, 5: LiF, 6: spinell

Viscosity

The viscosities of slags of both powders measured at 1300°C are very similar with 0.27 Pas for powder A and 0.26 Pas for powder B. The break temperature at 922°C of powder A is lower than the break temperature at 1020°C of powder B. The viscosities at break temperature are 4.65 Pas for powder A and 4.22 Pas for powder B. The slope of the viscosity versus temperature curve is steeper in case of powder B. The viscosity at 1100°C of powder A is 0.78 Pas while the viscosity of powder B is 1.58 Pas.

Characterization of the slag rims

Slag rim from mold powder A

The cross sections of the slag rims from powder A can be divided into three parts. On top and in contact with the mold powder which was not completely liquefied dominates the structure (see Fig. 5). From Table 3 it can be seen that the composition of this area 1 is in good agreement with the original powder. The observed phases are similar to the results from the quench tests. From the phase composition a temperature profile within the cross section maybe roughly

estimated. Contrary to the quench tests carbon is entrapped due to the rapid heating and the reducing atmosphere. The structure of area 1a, situated in the upper part of the slag rim next to the strand, correlates with the quench tests performed at 900°C and 1000°C, but the Al_2O_3 content is larger in case of the slag rim. From this, it can be concluded that as soon as there is any contact with the steel, the mold powder will change its composition.

At the bottom of the slag rim, solidified mold slag is present. From Table 3 it can be seen, that the composition of this area 3 largely deviates from the original mold powder. The Al_2O_3 content increased from 3.9 to 27.4 mass%. As a result, the SiO_2 content decreased from 44.2 to 25.1 mass %. Hence the C/S ratio increased. Phase I is the dominating solid phases (see Fig. 6). Between its crystals cuspidine and fluorite was formed.

Area 2 is situated between area 1 and 3. From Table 3 it can be seen, that the Al_2O_3 content is higher than that of the mold powder, but its level did not reach the level of area 3. It probably originated by the solidification of the molten powder and the modified slag. Noticeable are the spherical pores which result from the combustion of the entrapped carbon.

Table 3 Powder A: Chemical compositions determined by EDX of the slag rim areas distinguished

	F (mass%)	Na_2O (mass%)	MgO (mass%)	Al_2O_3 (mass%)	SiO_2 (mass%)	CaO (mass%)	MnO (mass%)	C/S	C/(A+S)
Area 1	12.9	13.3		3.9	44.2	20.1	5.6	0.45	0.42
Area 1a	12.2	12.3		11.1	37.6	22.2	4.7	0.59	0.46
Area 2	10.4	12.5	1.0	16.4	35.5	20.4	3.2	0.57	0.39
Area 3	10.3	12.9	1.0	27.4	25.1	22.0	1.4	0.87	0.42

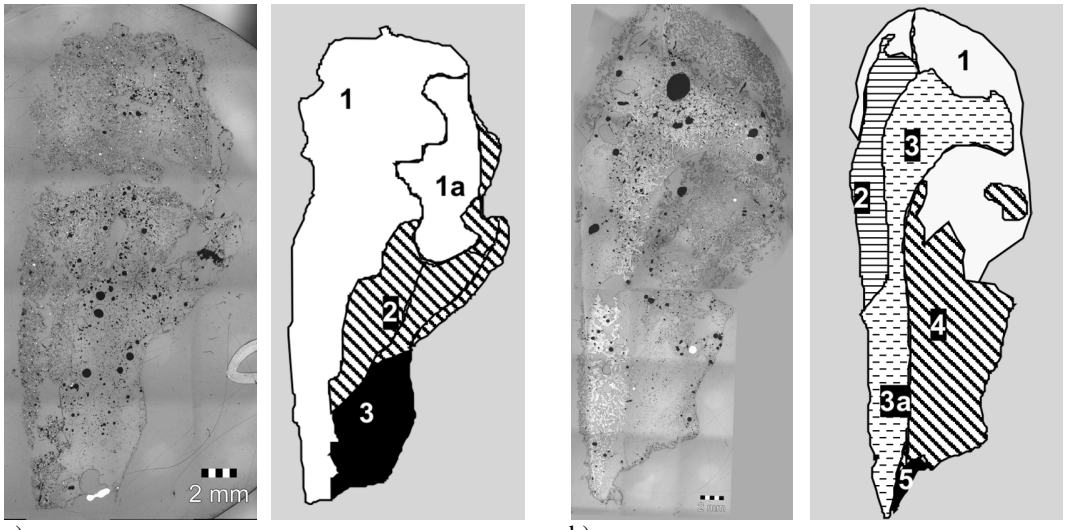

a) b)

Figure 5 Reflected light micrograph of the polished cross sections and areas distinguished, a) powder A, b) powder B

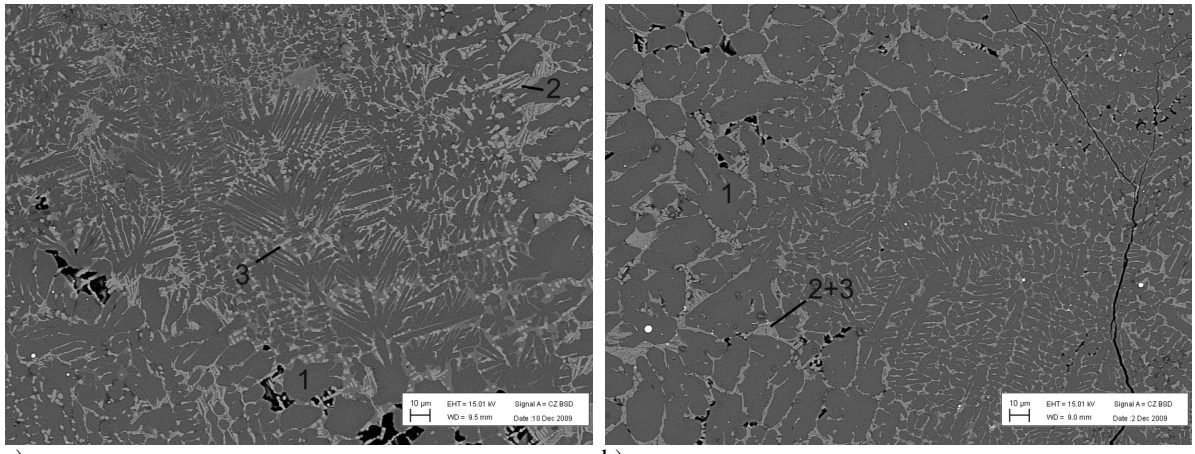

a) b)

Figure 6 Back scattered electron image of the crystallized modified slag at the upper part of the slag rim, a) powder A , area 3 b) powder B area 5, 1: phase I, 2: cuspidine 3: fluorite

Slag rim from mold powder B

In Figure 5 it can be clearly seen that the structure of slag rim from powder B differs from that of powder A. In contrast to powder A only the top and front of the slag rim is composed by mold powder which was not totally liquefied.

In contact with the mold, a mainly glassy layer with less than half of the Al_2O_3 content but higher amounts of SiO_2 and CaO compared to area 1 was formed (see Table 4).

Of particular interest is the occurrence of area 3. Remarkable is the high CaO content, although it is lower than that of area 2. It is mainly built of gehlenite, cuspidine and phase I (Fig. 7). It seems that this structure is only stable in a close temperature field. In the lower parts of the slag rim, the composition of this area is modified, but the characteristic gehlenite is still present. Spherical large pores due to the combustion of entrapped carbon are detected generally in this area.

Area 4 consists of solidified slag from the liquid pool and liquid original powder. Although the SiO_2 content of the powder was at a low level, the SiO_2 content of this area decreased to 14.4 mass%. In return, the Al_2O_3 content increased to 36.2 mass%. The microstructure is dominated by phase I (Fig.6). Depending on the position and consequently the temperature fluorite (at higher temperatures) and cuspidine (at lower temperatures) were formed in between. Small phases of NaF and due to the presence of Li, LiF occur, too.

Very similar is the structure of area 5. It is composed of solidified slag form the liquid pool and shows the highest Al_2O_3 content of this sample. Again phase I is the dominating crystal phase formed. In general the crystal size is smaller than in area 4.

Table 4 Powder B: Chemical compositions determined by EDX of the slag rim areas distinguished

	F (mass%)	Na_2O (mass%)	MgO (mass%)	Al_2O_3 (mass%)	SiO_2 (mass%)	CaO (mass%)	C/S	C/(A+S)
Area 1	14.6	14.0		28.3	21.8	21.4	0.98	0.43
Area 2	7.7	7.3	2.4	12.2	30.5	38.4	1.26	0.90
Area 3	8.9	7.3	1.5	27.4	22.6	32.2	1.42	0.64
Area 3a	12.6	12.3	1.1	33.4	15.6	25.1	1.6	0.51
Area 4	10.46	10.8	1.4	36.2	14.4	26.8	1.87	0.53
Area 5	10.9	6.7	1.3	28.9	12.9	25.3	1.96	0.62

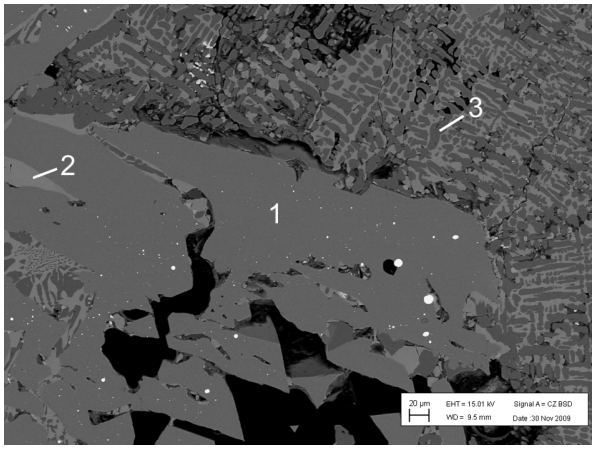

Figure 7 Back scattered electron image of area 3 from slag rim powder B, 1: gehlenite , 2: cuspidine, 3: phase I

Discussion

Comparing the results from mold powders and slag rims, it can be seen that the size of the upper slag rim part is mainly influenced by the melting and solidification behavior of the original powders. For both mold powders investigated, structures similar to the results from the quench tests were observed. Due to the lower melting temperature of powder A, the upper part of the slag rim is smaller in height and width than that of the slag rims generated with powder B.

Mold powder B has a high solidification temperature. It is most likely that due to the temperature variations caused by the oscillation, molten powder may solidify immediately due to the decreased temperature at the meniscus level during the downward mold motion. During the upward mold motion it will melt again. This cycling temperature may have caused an enhanced grow of gehlenite crystals. The crystallization of gehlenite causes a decrease of Al_2O_3 observed in area 2. From the composition it can be concluded that the middle section on the strand side of the slag rims (area 2 in case of powder A and area 4 for powder B) is not only formed by the painting mechanism reported by Perrot [4]. This region is more or less a mixture of molten powder and slag from the liquid pool. The solidification temperature of this mixed material is unknown, but should be higher in comparison to the molten powder because of its increasing C/S ratio and the increased Al_2O_3 content.

At the lower part of the slag rims, the Al_2O_3 content is increased with both mold powders. From the composition it is obvious that it was formed by the slag from the liquid pool on top of the steel meniscus. Due to the dramatic increase of Al_2O_3 of powder A, the structure of the solidified slag is similar to powder B in this region. The slag crystallized and formed phase I,

which is not mentioned in the literature so far. It seems that these phases belong to a solid solution with no fixed stoichiometry. Cuspidine, in general the dominant mineral phase with all fluor-containing powders, is present only between phase I at lower temperatures.

Carbon is entrapped in the slag rims of both mold powders. This carbon combusts later, but the formed carbon monoxide cannot escape through the viscous slag. As a result, pores are formed within the slag rim. Due to the earlier begin of melting of powder A (680°C) compared to powder B (933°C), more pores are present in case of powder A, because of powder B the temperatures were high enough for the carbon to combust before a cohesive liquid was formed by the other components. Due to its low contend carbon combustion nevertheless has a low impact on the slag rim size.

Conclusions

High Al_2O_3 contents and high C/S ratios of the mold powder lead to a higher melting and solidification temperature. As a result, the slag rim size, especially of the upper parts, will increase, with increasing alumina contents.

When casting high-alumina containing grades the mold slag composition can be significantly different from that of the original mold powder, even if the original mold powder has a very high Al_2O_3 content. Because of the lack of SiO_2, cuspidine is not the determining mineral phase with alumina based mold slags. Instead phases I will be formed.

Acknowledgments

The research program of the competence center “Advanced Metallurgical and Environmental Process Development” (K1-MET) is supported within the Austrian program for competence centers COMET (Competence Center for Excellent Technologies) with funds of the Federal Ministry for Transport, Innovation and Technology, the Federal Ministry of Economy, the province of Upper Austria and Styria, the Styrian Business Promotion Agency, of the Tyrol and the Tyrolian Future Foundation.

References

[1] A. Badri, T. T. Natarajan, C.C. Snyder, K. D. Powers, F. J. Mannion, M. Byrne, and A.W.Cramb, A mould simulator for continuous casting of steel: Part II. The formation of oscillations marks during the continuous casting of low carbon steel, *Metall. and Mat. Transa, B*, Vol 36B, 2005, p 373-383.

[2] J. Kromhout, R. Boom, M. Kawamoto, M. Hanao, *Proc. of the VIII International Conference on Molten Slags, Fluxes and Salts*, Santiago, Chile, 2009, p1041-1052

[3] C.-Å. Däcker, M. Glaes, S. P. Andersson, A. Salwén, C. Eggertson, Influence of slag rim formation on intial solidification of stainless steel, *Proc. of the 6th European Conference on Continoius Casting*, 2008, Riccione, Italy

[4] C. Perrot, J.N.Pontoire, C.Marchionni, M.R.Ridolfi, and L.F.Samcho, Several slag rims and lubrication behaviours in slab casting, *Proc. of the 5th European Continuous Casting Conference*, Nice, France, 2005, p 36-47

[5] K. Schwerdtfeger, Metallurgie des Stranggießens, *ISBN3-514-00350-5*, 1992, p 249-250

[6] I. Marschall, H. Harmuth, Investigation of slag rim growth in the continuous casting process, Proc. of the *Scanmet III*, Vol 2, Luleå, Sweden, 2008, p 419-425

[7] W. Wang, K. Blazek, A. Cramb, A Study of the Crystallization Behaviour of a New Mold Flux used in the Casting of the Transformation-Induced-Plasticity Steels, *Metall. and Mat. Transa, B*, Vol.39B, 2008, p 66-74